BACHELOR

The existence of a virtual anode inside a fusor

van den Beld, David H.T.

Award date:
2019

The Existence of a Virtual Anode inside a Fusor

D.H.T. van den Beld
1001770

Supervisors:
prof. dr. R.J.E. Jaspers
M. van Witsen

July 2, 2019

Abstract

Farnsworth-Hirsch fusors use an electric field to confine a plasma. Fusors accelerate ions, which in turn fuse if they have enough energy. These fusion reactions can produce neutrons, which can be used in cancer treatment.
Recent research found results of ion movement inside a fusor which oppose the common theory of fusor workings. Using Doppler spectroscopy, a radially outward acceleration has been measured. This does not comply with the traditional idea of the ions utterly being accelerated radially inward by the cathode inside the fusor.
This radial outward acceleration has been attributed to the hollow cathode effect giving rise to a virtual anode.
This experiment aims to proof or deny the existence of a virtual anode by measuring the ion velocity at different positions inside the fusor. A pressure of 0.2 Pa is used, which is significantly lower than in previous experiments.
Excited atomic hydrogen is created in charge exchange interactions between the accelerated ions and the background gas. As the excited atomic hydrogen gains the velocity of the ion in this reaction, the light emitted by the de-excitation of the excited atomic hydrogen shows a Doppler shift. This Doppler shift is measured and used to calculate the ion velocity at different positions in the star mode beam.
The fusor used in this experiment consists of two concentric shells. A voltage of 23 kV is applied to the cathode. The light emitted by the excited atomic hydrogen is captured using an optical set-up, designed by the author, which enables translation of the focus point in three directions.
The measured velocity profile shows an increase in ion velocity between the grid center and grid edge, proving the existence of a virtual anode.
It has been suggested that the strength of the virtual anode rises with the current in the plasma. Increasing the current by a factor of one hundred shows a steeper increase in ion energy. But as other variables were changed during this experiment, it cannot be conclusively stated that the strength of the virtual anode rises with the current.

Contents

1 Introduction

Nuclear fusion is often associated with energy generation, and there is good reason for this association. The ultimate goal of nuclear fusion is to create a reactor which can produce immense amounts of power [1]. At the moment the most famous fusion reactor is ITER, which is a giant tokamak [2]. Tokamaks use magnetic fields to confine the plasma required for nuclear fusion. Magnetic confinement, however, is not the only method used to confine plasmas. There is a class of machines known as inertial electrostatic confinement (IEC) devices, which use electric field to confine the plasma. In 1995 it has been proven that IEC devices are extremely unlikely to ever produce more energy than they require [3]. This is due to the fact that the power which has to be recycled in order to maintain the plasma is substantially higher than the fusion power. For this reason, IEC devices are most commonly used for other purposes. One of these purposes is the production of neutrons which can be used for the treatment of cancer [4].

The Farnsworth-Hirsch fusor is an IEC device which can be used for neutron production. The outer shell of the fusor is a grounded, spherical vacuum vessel. Inside this vacuum chamber a spherical grid is located, to which a high, negative voltage is applied. These two spheres function as anode and cathode respectively. If the voltage difference between the anode and cathode exceeds a value known as the breakdown voltage, the neutral gas in the device is ionized enough to sustain a plasma. Due to the voltage difference, the ions will be accelerated radially inward. The fusor is designed for two accelerated ions to collide in the center of the chamber. If their energy is high enough, they can fuse together. If the ions do not collide, they will move out the other side of the grid, and get pulled back in again, creating an oscillating motion. The fusion process is visualized in Figure 1.

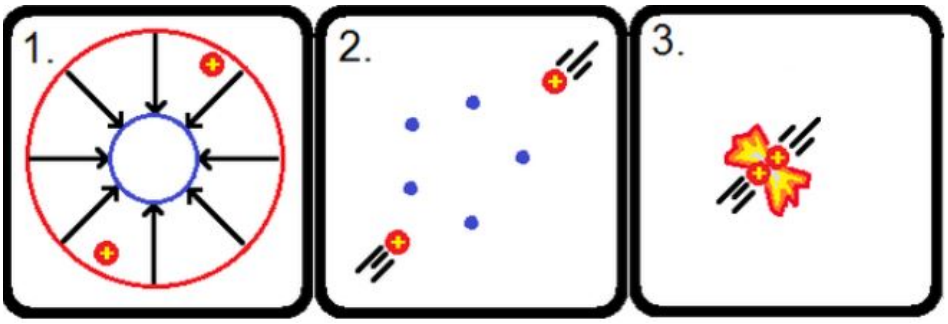

Figure 1: The basic fusion mechanism inside a fusor. (1) The fusor consists of two concentric shells, the cathode being inside the anode. Once a negative voltage is applied this creates a radially inward pointing electric field. (2) Positive ions are accelerated radially inward, the electric field speeds them up enough to meet fusion conditions. (3) Two ions collide, if their energy is enough, they fuse [5].

A suggested extension on this model of the fusor involves the hollow cathode effect [6]. The grid acts as a hollow cathode and a virtual anode is created in its center. The virtual anode is a consequence of a net positive charge being present in the center of the grid. Therefore the virtual anode causes the ions to be accelerated radially outward, rather than inward. It is suggested that the strength of the virtual anode scales with the amount of ions accumulated in the center of the grid. As this amount of ions increases with an increasing current, the strength of the virtual anode is expected to increase with an increasing current inside the plasma. The goal of this project is to prove the existence of a virtual anode and validate whether it increases with increasing current.
Researching the virtual anode is useful because, as of yet, fusors are not optimized to use the effect of a virtual anode in favour of neutron production. By gaining more knowledge about the virtual anode and its significance fusors might be optimized to use the virtual anode to increase neutron production.

The existence of a virtual anode has already been proven by research at the University of Sydney using a pressure of ≈ 1 Pa [7]. The experiments conducted during this project use a pressure of ≈ 0.2 Pa. As a lower pressure means a smaller amount of ions, the existence of a virtual anode at these lower pressures is investigated firstly. Afterwards, measurements for different currents are conducted which will determine the relation between the strength of the virtual anode and the current in the plasma.
The expected result of this project is to find a radial outward acceleration of the ions inside the grid, due to the virtual anode. This acceleration should increase when the current in increased. Outside the grid the ions are expected to be accelerated radially inward, due to the negative potential of the grid.

There is a lot of neutral gas present in the vessel. When ions collide with a neutral gas particle, there is the possibility of a charge exchange interaction, creating a fast excited atomic neutral. When this excited neutral decays it emits a photon, which is Doppler shifted due to the velocity of the excited neutral.
Using Doppler spectroscopy, the Doppler shift of excited neutrals is measured. This Doppler shift can be used to calculate the velocity of the excited neutrals. This velocity is the same as the ion velocity before colliding with the neutral [8]. By comparing the ion velocity at two different locations in the fusor it can be determined whether the ion has been accelerated or decelerated between the two points.

A new optical system has been designed by the author for the purposes of this project. This system achieves better accuracy of the location of measurement inside the fusor than could be achieved with previous experimental set-ups. Also, the new system allows for measurements to be reproduced reliably.

In this report, a theoretical background on the workings of both the fusor, and Doppler spectroscopy is presented in Chapter 2. Chapter 3 explains the experimental set-up used to conduct all measurements during this project. The design and calibration of the optical system is also discussed in this chapter. The results of these measurements are presented in Chapter 4, alongside a discussion of the reliability of these results. Chapter 5 concludes the experiments and compares the results with results found in other experiments. Suggestions for possible improvements which can be made in future projects are presented in chapter 6.

2 Theory

The goal of this project is to gain a deeper understanding of the ion movement inside a fusor. Therefore, the basic workings of a fusor are described in Section 2.1. Most theoretical models of a fusor do not include the hollow cathode effect, which might be responsible for ions moving in a different direction than previously believed. The hollow cathode effect is explained in more detail in Section 2.2.
The ion movement is measured using Doppler spectroscopy, which is explained in Section 2.3. These measurements result in spectra in which different peaks can be distinguished. These peaks are not only created by the Doppler shift of the measured light, but also by other physical effects. Section 2.4 discusses the analysis of the measured spectra and the significance of the other physical effects which are present in the spectra.

2.1 Fusor Physics

The Farnsworth-Hirsch fusor at Eindhoven University of Technology is a spherical fusor. An electric field inside it is created by applying a high negative voltage to a cathode grid, located in the center, while grounding the outer shell. This is also depicted in Figure 2. Inside the vacuum chamber a neutral gas is injected with a given pressure. As mentioned earlier a very common use of a fusor is neutron production, for which a deuterium gas is the most effective. In this project the neutron production is not relevant. Hence, a hydrogen gas is used, as this is chemically equivalent to deuterium for the purposes of this project.
Effects such as cosmic radiation cause the first ionisation inside the still neutral gas, creating an ion and electron. the electric field in the chamber causes the particles to be accelerated radially inward and outward respectively. When the electron hits a new neutral particle, another ion and electron pair is created. If each electron creates more than one ion, a breakdown is reached. Once this happens, a plasma can be sustained inside the chamber. The ions are accelerated radially inward till they get to the center, where they either collide and fuse, or fly out the grid and get pulled back by the electric field again. Colliding ions only fuse if they have enough energy to overcome the coulomb barrier. This energy is mainly kinetic energy, hence, the ion velocity inside the fusor is relevant when studying fusion inside a fusor.
Figure 3a shows the potential inside the fusor as described above. The potential is zero at the vacuum wall, denoted by R_v, and decreases to a value of $-V_c$ at the edge of the cathode. Here $-V_c$ is the (negative) voltage which is applied to the cathode. In the figure the radius of the cathode is denoted by r_c. Inside the grid the potential does not change, this can be understood from Gauss law for electric fields and the relation between the electric field and the potential.

$$\oint_A \vec{E} \cdot d\vec{A} = \frac{Q_e}{\epsilon_0} \tag{1}$$

$$\vec{E} = -\nabla V \tag{2}$$

In these relations the electric field is denoted by $\vec{E}$, the potential by V and the enclosed charge by Q_e. The vacuum permittivity is ϵ_0. If one visualizes a Gaussian surface within the grid, the enclosed charge Q_e is zero. From equation 1, and the electric field being isotropic, it follows that this requires the electric field to be zero. Substitution of a zero electric field into equation 2 yields a constant potential. An elaboration on this model is made in Section 2.2.
As can be seen in Figure 4a the plasma shows beams at the 'holes' in the grid. This is the so called star mode. The formation of these beams is an artifact of particles hitting the grid wires of the cathode and of an asymmetry in the potential. As the potential is applied to the grid wires, the potential in between the grid wires is slightly higher than at the location of the wires themselves.

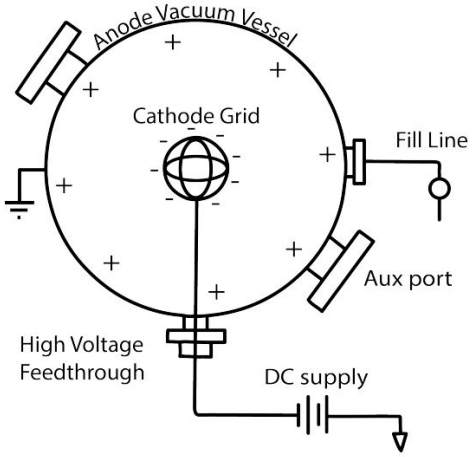

Figure 2: A schematic overview of a Farnsworth-Hirsch fusor showing the cathode inside the anode and two observatory ports, through which the inside of the fusor can be observed [9].

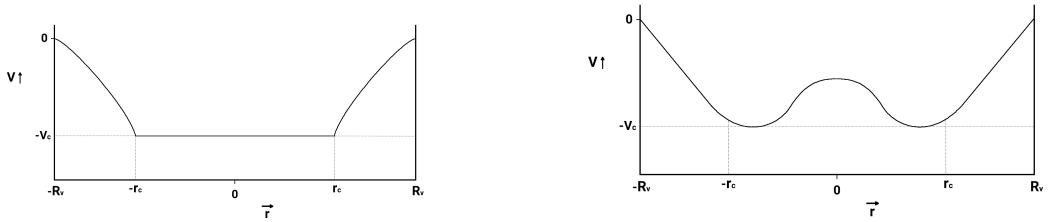

(a) The potential inside the fusor, the radius of the grid is denoted by r_c, the radius of the anode by R_v and the potential by V_c.

(b) The potential inside the fusor with the hollow cathode effect being taken into account. The height and width of the hollow cathode are not to scale.

Figure 3: The potential well in the fusor, left without and right with the hollow cathode effect taken into account.

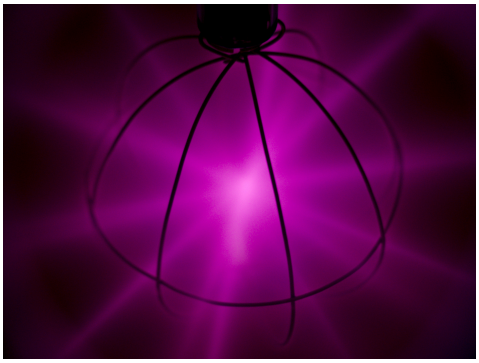

(a) The fusor operating in star mode. [10].

(b) The Nichrome grid with a radius of 4 cm, consisting of 5 wires.

Figure 4: The spherical cathode grid causes the fusor to show star mode beams when operating under certain conditions.

2.2 Hollow Cathode Effect

Recent research has found results showing the ion acceleration within the grid is radially outward [7] [11]. The electric field inside the fusor as described previously does not explain this acceleration. Kirpitidis et al. [6] suggest that this acceleration can be attributed to the grid acting as a hollow cathode. When ions strike the inside of the grid, they have the possibility to ionize the grid, creating a free electron. The electron is repelled away from the grid towards the other side of the grid, where it will again be repelled. This causes the electron to keep oscillating inside the grid, which is known as the pendulum effect. While oscillating back and forth, the electrons can either ionize background gas which is present inside the grid, creating more electrons and ions, or they can escape through the grid holes. As the electrons have a far higher velocity than the ions inside the grid they are more likely to leave through one of the grid holes, giving rise to a net positive charge within the grid. This positive charge forms a virtual anode which causes the ions to be accelerated outward. As the strength of the virtual anode scales with the amount of ions at the center of the cathode, it is expected that the strength of the virtual anode also scales with the current in the plasma. As this current scales with the amount of ions present in the plasma.

The addition of the hollow cathode effect changes the potential inside the fusor from Figure 3a to Figure 3b. As there is a virtual anode in the center of the grid, the enclosed charge Q_e in equation 1 is no longer zero. Hence, equation 2 no longer results in a constant potential.

The expected ion energy inside the cathode can be interpreted from Figure 3b. The positively charged ions will be repelled from the center of the virtual anode, being accelerated outward. The steeper the decrease in the potential, the bigger the acceleration, and thus the energy, of the ions. The resulting ion energy profile can be found by flipping Figure 3b vertically. Figure 5 shows the expected ion energies inside the cathode. As the height of the virtual anode is not known, Figure 5 is not drawn to scale.

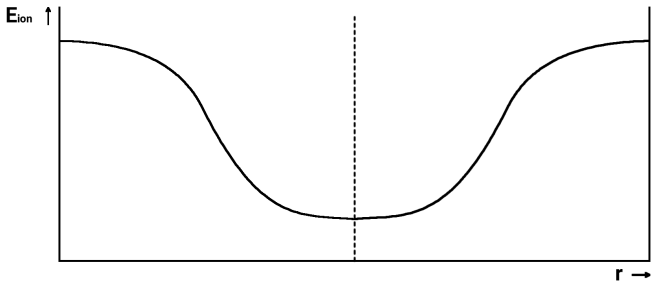

Figure 5: The expected ion energy inside the cathode, not to scale.

2.3 Doppler Spectroscopy

As the charged ions move through the chamber, there is a chance for them to collide with the background gas. As the plasma originates from a hydrogen gas, the ions which are present are H^+, H_2^+ and H_3^+. The background gas consists of H_2, with small amounts of H and H_3. As the background gas only has small amounts of the later two molecules, collisions involving either H or H_3 are neglected [12]. When an ion collides with the background gas there is a possibility for a charge exchange interaction.

The different ions each cause a different charge exchange interaction [13]

$$H^+ + H_2 \rightarrow H^* + H_2^+ \tag{3a}$$
$$H_2^+ + H_2 \rightarrow H^* + H_2^+ + H \tag{3b}$$
$$H_3^+ + H_2 \rightarrow H^* + H_2^+ + H_2, \tag{3c}$$

with H^* denoting an excited atomic hydrogen particle. The energy in each of these interactions is provided by a different parent ion with a different weight. The energy of the parent ion is divided equally between the individual hydrogen atoms of the parent ion [12]. Therefore, the energies of the H^* originating from H_2^+ and H_3^+ are respectively only half and one third of the energy of the H^* originating from H^+. Therefore, the excited neutrals originating from the heavier parent ions have a lower velocity.
When the excited atomic hydrogen falls back to its ground state, it emits a photon at a known wavelength of 656.280 nm [14], also known as the Balmer-alpha line. Due to the velocity of the neutral, this photon has a Doppler shifted wavelength which can be quantified using

$$\Delta\lambda = \frac{v\lambda_0}{c} \cdot cos\phi, \tag{4}$$

with v being the velocity of the neutral, λ_0 the Balmer-alpha wavelength, ϕ the angle between the directions of the neutral and photon and $\Delta\lambda$ the shift in wavelength due to the Doppler effect. This equation assumes that relativistic effects can be neglected, which holds in the regimes analyzed in this project. Substitution of $E_{kin} = mv^2/2$ into equation 4 gives the equation for the kinetic energy of the neural in terms of the Doppler shifted wavelength

$$E_{kin} = \frac{mc^2(\Delta\lambda)^2}{2\lambda_0^2 cos^2\phi} \tag{5}$$

where m is the mass of the neutral and E_{kin} the kinetic energy.
The Doppler shifts can be used to determine the direction of the neutral velocity. A red-shifted peak, having a wavelength above the Balmer-alpha wavelength, means that the particles creating this peak are moving away from the spectrometer. Whereas a blue-shifted peak means that the particles are moving towards the spectrometer.
As all peaks measure light emitted by atomic hydrogen, the parent ions will be used to refer to the different Doppler shifted peaks.

2.4 Spectral Analysis

The spectrum of the light coming from a star mode beam is expected to show a Balmer-alpha line and three Doppler shifted lines corresponding to the different charge exchange interactions as described in equation 3, this spectrum is shown in Figure 6. The three peaks originating from the different ions can be observed on both sides, meaning that the ions move in both directions. H^+, H_2^+ and H_3^+ all get the same energy in the fusor, but in the charge exchange interaction the energy of the ion is divided equally among the hydrogen atoms in the ion. Therefore, the ratio of the three Doppler shifts can be determined using equation 5.
From previous experiments it is known that the peaks from H_2^+ and H_3^+ are bigger than the peak from H^+ [7] [11], this can also be seen in Figure 6.

Figure 6 shows peaks in the spectrum, rather than spectral lines at the Doppler shifted wavelengths. This is an artifact of multiple processes which cause the spectral lines to broaden. The significance of these broadening processes is investigated by comparing them to the expected distance between two of the Doppler shifted peaks. If the Doppler shifted peaks overlap due to the broadening effects this needs to be taken into in later analysis.

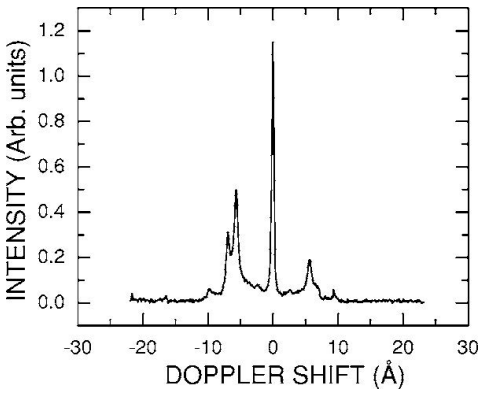

Figure 6: The expected spectrum, showing the Balmer-alpha peak and three Doppler shifted peaks originating from the different ions [11].

From equation 5 it can be seen that the peaks from H_2^+ and H_3^+ are closest together, which is why the distance between these two peaks is compared with other spectral broadening effects. The difference between the Doppler shifts of H_2^+ and H_3^+ is estimated for an ion energy and angle ϕ which are typically used during the measurements. These values are 20 KeV and 130° respectively. This results in respective Doppler shifts of $\approx$ 2nm and $\approx$ 1.5 nm for H_2^+ and H_3^+. This means that peaks are expected to be $\approx$ 0.5 nm apart.

2.4.1 Thermal Doppler Broadening

Thermal Doppler broadening is a result from the random thermal motion of particles. The instantaneous velocity due to thermal motion of an excited neutral at the moment of falling back to its ground state should be added to the velocity of the particle gained as an ion due to the electric field. This causes the particles to have a Gaussian distribution around the Doppler shifted wavelength, instead of showing one line. The full width half maximum due to this effect is

$$\Delta\lambda_{TDB} = \lambda_0 \sqrt{\frac{8K_bT}{mc^2} ln2}, \tag{6}$$

with T the temperature, λ_0 the spectral line wavelength, m the mass of the particle, $\Delta\lambda_{TDB}$ the full width half maximum due to thermal Doppler broadening and the rest of the variables constants of nature. For an H_3 particle with a temperature of 1000 K this gives a full width half maximum of 0.01 nm. As the different peaks originating from the different charge exchange interactions described in equation 3 are separated by $\approx$ 0.5 nm they will not overlap as a consequence of thermal Doppler broadening. Therefore this effect is neglegible.

2.4.2 Star Mode Beam Divergence

During the measurements the star mode beam is observed under an angle ϕ, this is the angle between the star mode beam and the path of the photon. This is equivalent to the angle between the star mode beam and the optical path. From Figure 4a it can be seen that the star mode beam diverges. For this reason, the velocity vector of most particles in the beam does not exactly make an angle of ϕ with the optical path, but an angle which differs slightly. So when measuring at ϕ_1, light coming from particles traveling between angles $\phi_1 - \delta\phi_1$ and $\phi_1 + \delta\phi_1$ is also measured.
This deviation $\delta\phi_1$ is estimated to be $\approx 5°$. Using equation 5 this corresponds to a deviation in the Doppler shifted wavelength of $\approx$ 0.2 nm. This value is slightly lower than the expected separation

of the different peaks, which is 0.5 nm, but the effect of the diverging beam should be kept in mind during analysis of the results.

2.4.3 Instrumental Broadening

As the spectrometer is not perfect it causes broadening of the peaks in the spectrum. In order to investigate whether this effect is significant a calibration has to be carried out. This is described in Section 3.5.

2.5 Relevant Length Scales

Once excited atomic hydrogen is created in a charge exchange interaction, it does not emit a photon instantaneously. The lifetime of atomic hydrogen depends on the atomic sublevel which causes the Balmer-alpha decay. The lifetimes are in the order of 10^{-8} s [15], meaning that a fraction of $1 - \frac{1}{e}$ ($\approx$ 63 %) has decayed after this time. Ion velocities during this experiment are typically 10^6 m/s, which is calculated for a H^+ ion using a cathode voltage of -23 kV. Multiplying the lifetime and typical velocity gives the average distance travelled of an excited neutral before emitting a photon. This distance is 1 cm. As the excited neutral is not charged, it is not accelerated over this distance.

As explained previously, the ions are expected to be accelerated radially outward by the virtual anode. But, while being accelerated the ions can collide with other particles, meaning that they are not accelerated to their maximum velocity. In order to check whether this effect is significant, the mean free path of the ions is calculated using

$$\lambda_{mfp} = \frac{1}{\sigma n}, \tag{7}$$

with σ being the charge exchange cross section ($\approx 10^{-19}\ m^2$) [16] and n the ion density. Using the ideal gas law to calculate the ion density n a mean free path of $\approx$ 10 cm is found. This means that most ions are free to accelerate over the full distance between the cathode center and cathode edge.

3 Experimental Set-up

This chapter will start with a more detailed description of the TU/e fusor in Setion 3.1. Section 3.2 will explain the design and calibration of the optical set-up used to measure the spectra, the experimental procedure used to obtain these spectra is clarified in Section 3.3. Sections 3.4 and 3.5 discuss different calibrations which were required before the actual measurements could be conducted.

3.1 The TU/e Fusor

All measurements conducted during this project use the fusor at Eindhoven University of Technology. This is a spherical fusor with an inner radius of 25 cm. For stability the spherical vacuum chamber is mounted in a metal case, surrounded by a wall of plastic material with a width of 10 cm which acts as a neutron shield.
While operating, the pressure in the vacuum chamber is regulated using a Pfeiffer Vacuum HiCube pump in combination with a Pfeiffer Vacuum HiSpace 80 1500Hz turbo pump. The outflux of gas is regulated using a Pfeiffer Vacuum EVB 063 SA valve and the gas inlet is regulated by a Pfeiffer Vacuum EVR 116 valve. These components are controlled using a Vacuum RVC-300 controller. This controller is in turn operated by the user, using a Matlab GUI created by a student of the TU/e.
The cathode is a spherical grid made from Nichrome with a diameter of 4 cm, it is made out of 5 wires as shown in figure 4b. The cathode is suspended in the vacuum chamber using a stalk, which is in turn connected to the Heinzinger HNCs DC power supply. This power supply can provide a current of 100 mA and a voltage of 120 kV. In order to ensure the safety of the fusor operators there are multiple precautions installed. Before the high voltage supply can be switched on a fence first has to be closed and the door of this fence has to be barred, ensuring that people cannot reach the fusor once the high voltage supply is switched on.
On the vessel there are ports through which the inside of the vessel can be observed, these observatory ports are at 45° angles as measured from the horizontal. Light exiting the chamber through one of these ports is caught by an optical setup and redirected into an Andor Shamrock 500i spectrometer. These are described in more detail in Section 3.2.
As a fusor can be used for neutron production, there are multiple neutron counters placed inside the room, but as the measurements in this project are all conducted using hydrogen gas, this is not described in any further detail.

3.2 Optical Set-up

The spectrum inside the fusor is measured using an Andor Shamrock 500i spectrometer. An optical fiber is used to direct the light from the plasma into the spectrometer. In order to focus the optical path traced by the fiber a new optical set-up is required. This optical system is designed and calibrated by the author, the design and calibration are discussed below.

3.2.1 Design of Optical Set-up

Measuring the ion velocity at different positions in the star mode beam is done by measuring a spectrum at the different positions. An optical set-up is used to fix the location in the beam where the spectrum is measured, meaning that only the light from the location chosen by the operator will be captured by the optical fiber. The location of the beams in the vacuum vessel is determined by the position of the grid, this position is usually changed when a new grid is suspended in the vacuum chamber. To deal with this problem an optical set-up is required that can translate the focal point in three directions, this optical set-up is shown in Figure 7a. In the figure, the light coming from the plasma has to be focused on the optical fiber, which is the observer in the figure. The light first falls onto a mirror (PF10-03-P01), which can be rotated to fascilitate translation of the focal point in the x-, and y-direction as given in Figure 7. Afterward, the light falls onto a planar-convex lens with a focal length of either 400mm (LA-1172-A) or 500mm (LA-1908-A), sliding this lens along the optical

rails in the y-direction fascilitates translation of the focal point in the z-direction. Lastly, the now parallel light falls onto a convex-planar lens with a focal length of 25.4mm (LA-1951-A), which focuses the light onto the optical fiber holder.
In order to collect light from the fusor the optical system is mounted on one of the observatory ports on the fusor, as shown in Figure 8. The optical system is mounted at a fixed position, this ensures the reproductability of the measurements.

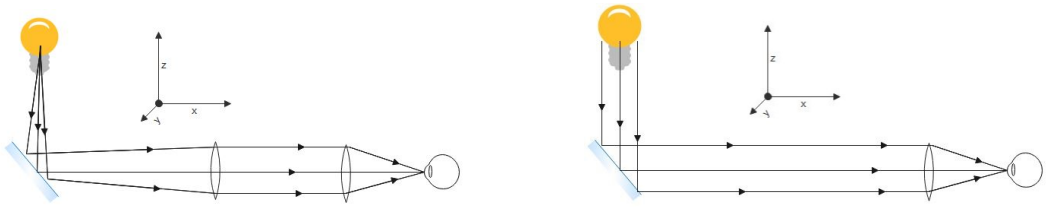

(a) The optical set-up with a lens to create one focus point

(b) The optical set-up with the left lens removed, now measuring parallel light.

Figure 7: The two optical set-ups created to aim the location at which spectra are measured

The spectrum is measured using an Andor Shamrock 500i spectrometer, which has an aperture of F/6.5 [17]. Meaning that only light with an angle of incidence less than $\approx 4.4°$ will be received by the entrance mirror in the spectrometer and displayed in the measured spectrum. The light is transmitted into the spectrometer using an optical fiber. To achieve a clear spectrum, the entirety of the entrance mirror should be illuminated by the optical fiber. Therefore the optical fiber needs an acceptance cone of atleast 4.4°. The optical fiber used in this experiment has a numerical aperture of 0.39. The numerical aperture is defined as $NA = n_1 sin(\theta_1)$, with θ_1 the angle between the maximal angle of incidence and n_1 the refractive index of the material in which the light travels. Inside the spectrometer the light travels in air, so $n_1 \approx 1$ and therefore the maximal angle of incidence is $\approx 23°$. This means that an optical fiber with a numerical aperture of 0.39 is good enough to transmit a maximal signal to the entrance mirror in the spectrometer.

3.2.2 Position Calibration of Optical Set-up

In order to be able to aim the focus point of the optical set-up at a specific position in the star mode beam, a position calibration of the optical set-up has to be done. The goal of this calibration is to determine a relation between the displacement of the mirror in the optical system and the location of the focus point in the star mode beam.
Translation of the focus point in the x-, and y-direction is done by rotating the mirror in the same directions. The mirror is rotated by turning the nobs which are assembled onto the mirror. The first step in calibrating the set-up is calculating the displacement of the focal point in terms of the amount of rotations of the nobs. This was done by mounting the set-up onto an optical table. Then, the nobs were turned and the displacement of the focal length was measured, from these results the angular displacement was calculated.
The location of the beams is determined by taking a picture through the observatory port when the fusor is operating in star mode. Figure 9 shows the location of the particular star mode beam with respect to the optical path. The angle α can be determined from the picture and the distance from the optical system to the grid center is a known constant. The distance between the focus point and the grid center can be chosen for each individual measurement. With these known variables, the angle ϕ can be determined. In Section 4.2 a calculation of the energy of a H^+ ion is presented, in this calculation ϕ is determined for a specific measurement.
It was also tried to make a theoretical calculation of the location of the star mode beam, but the as-

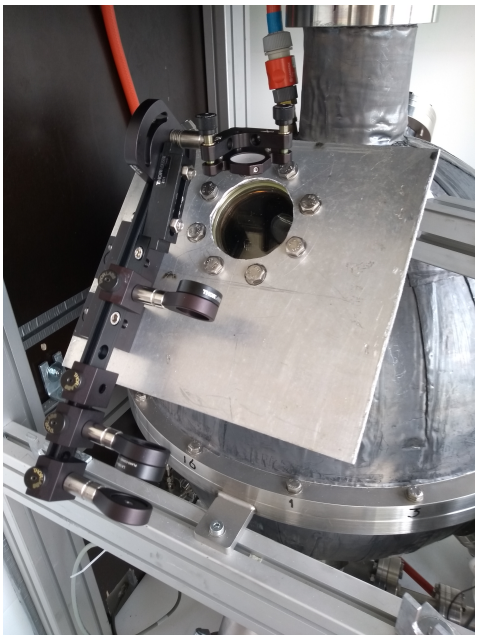

Figure 8: The optical system mounted on the fusor observatory port

sumptions required to make this calculation made it far less accurate than the method using a picture. As the location of the focus point of the optical system and the star mode beam are now determined, the position of the focus point can now be expressed in terms of rotations of the two nobs on the mirror. Figure 10 shows a the amount of rotations needed on the nobs responsible for the horizontal and vertical displacement to get the focus point to a certain position in the star mode beam.

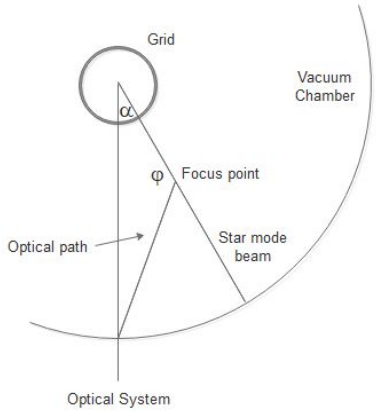

Figure 9: A sketch showing the location of the star mode beam, the optical path and the angle ϕ used in equation 5.

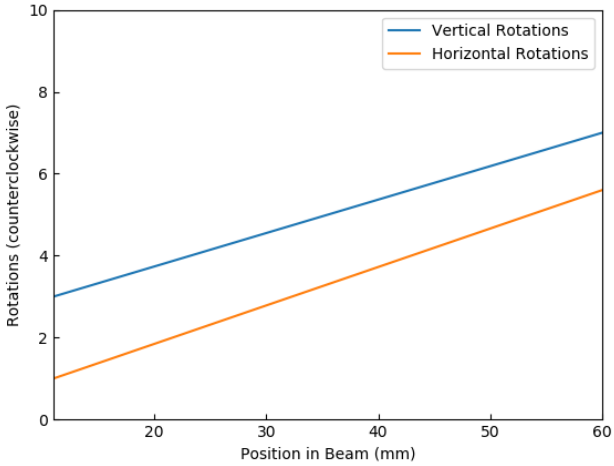

Figure 10: The calibration of the optical system. Once a position in the beam is chosen, the rotations required to move the focal point to this locations can be seen on the vertical axis.

During the calibration of the optical system it was noticed that aiming the focus point in the beam was not always successful. This was noticed due to the measured spectra showing lower photons counts than expected. This is attributed to a few causes which cumulatively resulted in an error that was often too big to aim in the star mode beam.
The grid often started shaking during the measurements, more on this will be explained in Section 3.3. Even though this effect was minimalised, it might have resulted in the grid being displaced slightly with respect to its position on the picture which was used to locate the beam.
The nobs on the mirror do not have any tick marks on them, making it hard to precisely rotate the nobs a given amount. Measuring the distance of the screw connected to such a nob would be a possibility to make the rotations more accurate, but this is not possible as the screw can not be accessed when the optical system is mounted on the fusor.
To account for these errors, the left most lens in Figure 7a was removed, creating the optical system as shown in Figure 7b. The new optical system will catch light coming from a bigger part of the vacuum chamber, but it only catches light which falls onto the lens perpendicularly. The main advantage of this system is that it is easier to aim the focus point at the star mode beam, as the focus point is now the same size as the lens. The main disadvantage is that the previous system caught light coming from the focus point under a certain angle, while the new system only catches the light falling perpendicularly on the lens.

3.3 Experimental procedure

A clear star mode with high voltages is expected to give the best results. A clear star mode will make it easier to aim the focal point in the beam and a high voltage will give the ions a higher velocity, and thus a bigger Doppler shift. The TU/e fusor is connected to an ion source, which enables the fusor to operate at pressures which are normally below the Paschen curve. The extra ions make it possible for a discharge to be sustained. Operating at lower pressures means that the voltage will increase, which is beneficial for the spectral measurements.
Before using the ion source, it was investigated whether the use of the ion gun would have any other effects on the measurement, beyond enabling the fusor to operate at low pressures. This was done by measuring at higher pressures, where the ion source was not required. At those pressures, the spectrum was measured once with the ion source being used, and once without it. The voltage was

kept as equal as possible during these two measurements, meaning that differences in the spectra were solely an effect of the ion source. These measurements were done for multiple pressures at multiple locations. Figure 11 shows the spectrum at a location about 2 cm outside the grid. As can be seen from the figure, the addition of the ion source increases the Doppler shifted peak significantly, the same conclusion was drawn from all other measurements. For this reason the ion source is not used during the rest of the measurements.
For the actual measurements, the pressure was made as low as possible while still sustaining a discharge. This resulted in the grid shaking due to the high voltages. Increasing the pressure, and thus decreasing the voltage, minimized the grid from shaking. This resulted in a pressure of 0.19 Pa, a current of 29 mA and a voltage of 23 kV.

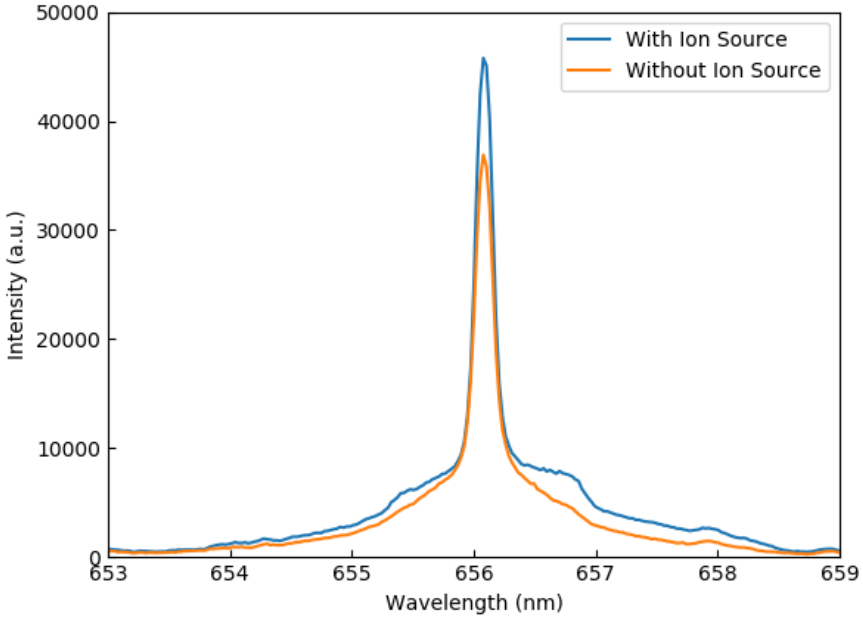

Figure 11: The spectrum when using the ion source with a current of 0.6 mA and a voltage of 0.57 kV and without using the ion source.

3.4 Calibration of the Spectrometer

A spectrometer splits light into its different components, and outputs a spectrum showing the relative presence of each component based on the intensity of this component [18]. When the light is split each different wavelength is focused on a specific pixel inside the spectrometer, the signal from these pixels is translated into a spectrum. Calibration of a spectrometer assigns a wavelength to each of the pixels, ensuring that the signal received by the pixels is properly translated to a spectrum displaying wavelengths.
The calibration of the spectrometer was done by measurement of a hydrogen plasma in the fusor. This plasma will emit light at the Balmer Alpha and Beta lines, which have known wavelengths of 656.280 nm and 486.231 nm respectively. [14] The pixels at these wavelengths will show an intensity peak, and thereby the calibration software in the spectrometer can be used to assign the known wavelengths to these pixels. It should be noted that in this experiment the spectrometer had pre-installed settings

assigning the Balmer Alpha line to 656.0 nm, these settings could only be overruled by a calibration for each individual measurement.

3.5 Calibration Instrumental Broadening

As the spectrometer is not perfect, it shows spectral lines as Gaussian peaks in the spectrum. If the spectrometer broadens the peaks too much, they start overlapping, which can result in the data being impossible to interpret. Therefore, the spectrum of a helium-neon laser with a known wavelength of 633 nm was measured. This spectrum shows a gaussian peak around this wavelength as shown in figure 12. The full width half maximum of this peak is ≈ 0.15 nm.
In section 2.4 it was estimated that the different peaks will be ≈ 0.5 nm apart, meaning that the instrumental broadening alone will not cause the peaks to overlap. But, when using lower voltages the effects of instrumental broadening should be kept in mind, as the peaks are expected to be closer together at lower voltages. Also, the instrumental broadening should be used to calculate the cummulative broadening of all spectral broadening processes, this is done in Chapter 4.
The helium neon laser used in this calibration was not aimed at the spectrometer directly. A light diffuser was used to ensure that the laser did not damage the spectrometer.

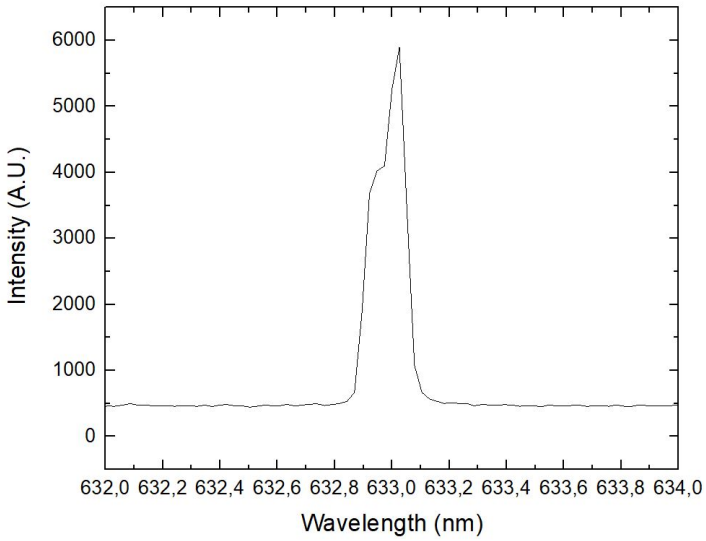

Figure 12: Spectrum measured by the spectrometer of a helium neon laser with a wavelength of 633 nm, showing the magnitude of the instrumental broadening of the spectrometer.

4 Results and Discussion

In this chapter the measurement results are presented and their validity is discussed. Section 4.1 explains how the Doppler shift is determined from the raw data. In Section 4.2 the energy of a H^+ ion located at 11 mm from the grid center is calculated. In Section 4.3 the ion velocity at different locations in the star mode beam is presented, and possible explanations for the velocity profile are given. Section 4.5 discusses the validity of the measurements and presented data.

4.1 Spectral Analysis

The spectrum at multiple positions in the star mode beam is measured using the fusor settings as described in Chapter 3. All data is acquired from measurements in the star mode beam whose location is specified in Section 3.2.2. The measurements were conducted using a pressure of 0.19 Pa, a current of 29 mA and a voltage of 23 kV.
Figure 13 shows the data measured at $\approx$ 11 mm in the beam, this is the distance between the grid center and the location of the measurement. From Figure 13 it can be observed that there are Doppler shifts to both sides of the spectrum.
From Section 2.3 it follows that a blue shift is expected. The virtual anode accelerates ions which are created inside the cathode radially outward. Some of these ions pass through the grid, so radial outward motion is expected both inside and outside of the grid. This radial outward motion creates a blue shift in star mode beams coming towards the spectrometer. In Section 2.1 it is explained that ions which are created outside the grid are accelerated radially inward. A share of these ions passes the grid wires, meaning that radial inward motion is to be expected both inside and outside the grid. This creates the measured red shift.
The spectrum in Figure 13 does not show distinct peaks as described in Section 2.4. As the Doppler shifted wavelengths cannot be obtained from Figure 13 directly, an algorithm is written which uses a non linear least squares fit method to determine the different Doppler shifted peak. This algorithm approximates the peaks originating from different charge exchange interactions as Gaussian peaks. In order to make the fit as trustworthy as possible, multiple physical relations were included in the algorithm. These physical relations will be discussed below.

Firstly, the maximal Doppler shifted wavelength of the H^+ ion is calculated. In Figure 13 a voltage of 23 kV was used and the angle between the ions and the optical path was 134°. Using equation 5 this results in a Doppler shift of $\Delta\lambda_{max} \approx 3.2$ nm. Thus, a lower and upper bound of 656 $\pm$ 3.2 nm are used.
Secondly, previous experiments state that it is often not possible to distinguish the H_2^+ and $_3^+$ peaks from each other, as they overlap too much [11] [19]. This problem can be solved by approximating both these peaks as one peak, referred to as the $H_{2.5}^+$ peak.
Thirdly, the Doppler shifted wavelengths of H^+ and $H_{2.5}^+$ have a known ratio. The ions which create the excited neutrals all have the same energy, and divide this energy equally between the hydrogen atoms in the ion during the charge exchange interaction. This results in the excited neutrals originating from $H_{2.5}^+$ to have an energy which is a factor 2.5 lower than the energy of the excited neutrals originating from H^+. This ratio is implemented in the algorithm, meaning that only the Doppler shift of the H^+ is left as a free parameter.
Fourthly, an extra peak is incorporated in the algorithm. This peak represents light coming from neutral which were created by slower ions. These slow ions have energies which are significantly lower than the energy of the H^+ ion, hence the Doppler shift of this peak is bound to a maximum value of 0.5 nm.
Fifthly, it is known from literature that the H_2^+ and H_3^+ peaks are more intense than the H^+ peak [19]. This can also be seen in Figure 6. Therefore, the intensity of the $H_{2.5}^+$ peak is set to be atleast four times the intensity of the H^+ peak. Also, the ratio between the slow ion peak intensity and the H^+ peak intensity is similar for both the red and blue shifted peaks.

Lastly, the standard deviation of the peaks is estimated using values found in Section 2.4. Addition of all the broadening effects gave a standard deviation of 0.35 nm. The upper bound for the standard deviation in the algorithm is higher to account for effects which were potentially neglected. Also, the standard deviation of the $H^+_{2.5}$ peak has an upper bound which is doubled, as this peak is expected to be significantly broader.
The resulting fit to the data represented in Figure 13 is shown in Figure 14. The different Gaussian peaks are shown to make the figure more insightful.
As the location of the $H^+_{2.5}$ peak is fixed with respect to the H^+ peak, only the Doppler shift of H^+ as calculated by the algorithm will be used in further analysis.

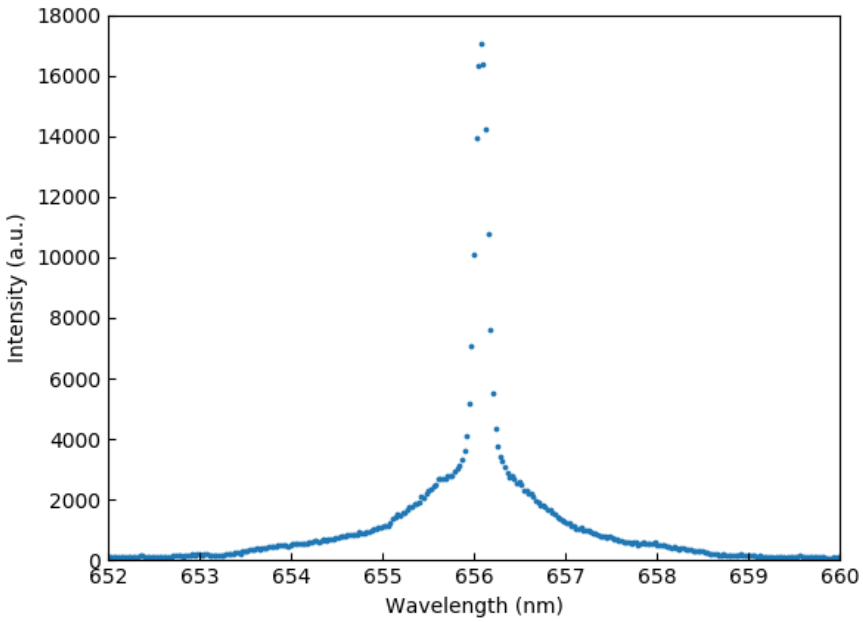

Figure 13: The spectrum measured inside the star mode beam 11 mm away from the grid center.

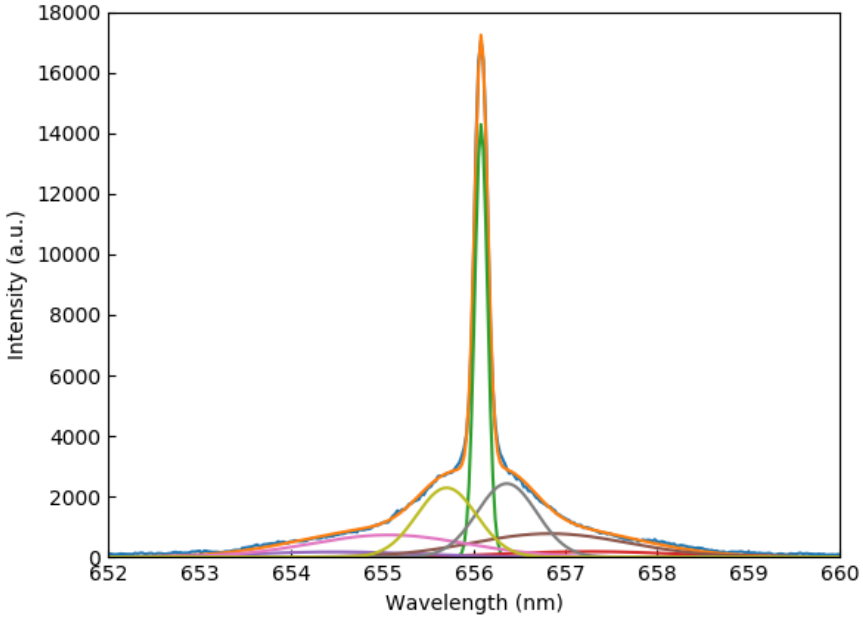

Figure 14: Different Gaussian peaks fitted to the data measured in the beam at 11 mm using the algorithm as described in the text.

4.2 Energy of the H^+ ions

The energy of the H^+ ions can be calculated using equation 5. In this equation, the variables still required are ϕ, $\Delta\lambda$ and m. This section will show the calculation of the energy of the H^+ ion in the star mode beam 11 mm away from the center of the grid. The calculation is analogous for other locations, and for the energy of other ions.
The mass m of the H^+ ion is 1 amu, or $1.6605{\cdot}10^{-27}$ kg. The Doppler shifted wavelength of the excited neutral created in a charge exchange interaction with the H^+ ions is calculated by the fit. At a distance of 11 mm from the grid center this value is $\Delta\lambda = 1.24$ nm.
The angle between the star mode beam and the optical path of the light falling onto the optical fiber is denoted by ϕ, as shown in Figure 9. The angle ϕ can be calculated by using the law of cosines

$$a^2 = b^2 + c^2 - 2 \cdot b \cdot c \cdot cos(\alpha) \tag{8}$$

two times. The first time the known distance between the grid center and the mirror in the optical system, and the known distance between the grid center and the focus point of the optical system are used in combination with the angle between them to obtain the distance between the focus point and the mirror.
Using the law of cosines again, this time with ϕ being the target variable, yields $\phi \approx 134°$.
Substitution of ϕ, $\Delta\lambda$ and m into equation 5 results in the energy of the H^+ ions in the star mode beam 11 mm away from the center. This energy is 5.2 KeV. The uncertainty of this result will be discussed in Section 4.5.

4.3 Ion Velocity in the Star Mode Beam

In order to find the velocity of the ions along the entire star mode beam, spectra are measured at different positions in the beam. These spectra are shown in Figure 15. In this figure, the Doppler shift

becomes less as the distance in the star mode beam increases. But for each measurement the angle between the optical path and the star mode beam, ϕ, also decreases. For this reason, the decreasing Doppler shift does not mean that the ions are moving slower as they get further in the beam.
The Doppler shifted peak corresponding to the H^+ ions is obtained using the same fit as used in Figure 14. For each of these blue Doppler shifts, the energy of the ions has been calculated using the calculation as explained in Section 4.2. The resulting energies are shown in Figure 16.
In Figure 16 the cathode edge is represented by a line at a distance of 4 cm from the cathode center. It can be seen that the ion energy is increasing slightly from the cathode center to the cathode edge, but as the error bars indicate this result is not trustworthy.
Once the ions have passed the grid Figure 16 shows a more conclusive decrease in ion energy. This decrease can be explained using Figure 3b. As the ions are positively charged, they are attracted by the negatively charged cathode once they are in between the grid and outer wall.
In order to get more conclusive results regarding the ion energy inside the cathode, experiments were conducted using a higher current.

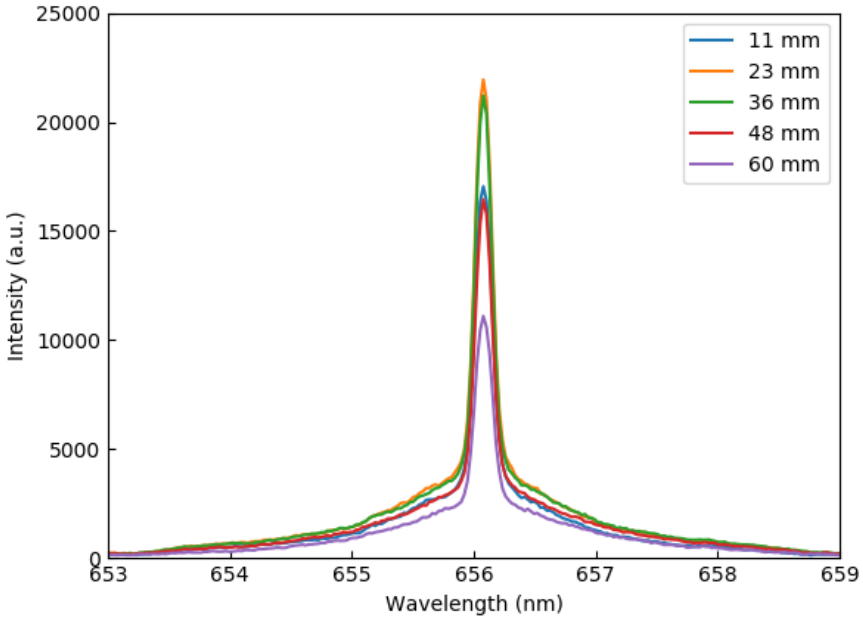

Figure 15: The measured spectra at different positions in the star mode beam.

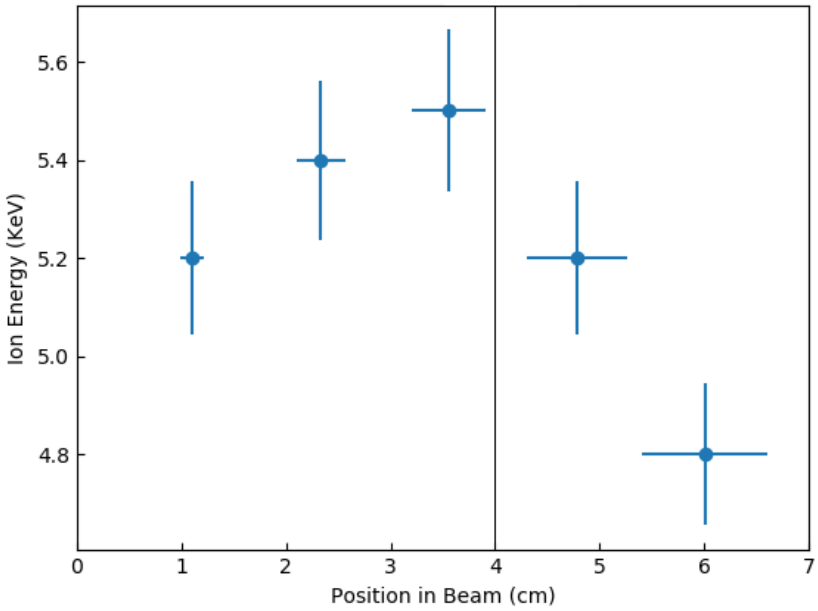

Figure 16: The energy of H^+ ions at different positions in the star mode beam, the cathode edge is located at 4 cm (note that the vertical axis does not start at zero).

4.4 High Current Regime

Measurements using higher current are conducted as it is theorized that a higher current will lead to a stronger virtual anode, this is explained in more detail in Section 2.2. The high current measurements are expected to create a steeper increase in ion energy inside the cathode, from which a more conclusive answer to the research question can be drawn.
The higher current is supplied using a different power supply unit specially designed for the TU/e fusor [16]. This power supply unit delivers power to the cathode in pulses. The pulsed power means that overheating is less of a problem, so higher currents can be reached without any damage being done to the equipment.
Figure 17 shows the spectrum measured at 23 mm in the star mode beam, using a current of 2 A. Measurements at different positions in the star mode beam show similar spectra. The spectra are analyzed by the same method as used in the lower current regime. The resulting fit is shown in Figure 18. The Gaussian peak corresponding to the blue shifted H^+ is used to calculate the H^+ energy at the different positions in the star mode beam, the resulting energies can be seen in Figure 19. During the high current experiments, a pressure of 0.37 Pa was required to sustain a plasma, while a pressure of 0.23 Pa was used during the low current measurements. This higher pressure results in more ions being present during the high current experiment, so an increase in ion energy cannot be solely attributed to the higher current.
Figure 19 shows a clear radially outward acceleration of the ions inside the grid. It can be seen that the ion energy is higher when using a higher current. Also, the increase in ion energy is about 2 KeV when using a current of 2 A, whereas this is only about 0.3 KeV when using a current of 20 mA. Thus, the ion energy increases by about a factor of ten when increasing the current by a factor of 100. But, as this increase in ion acceleration is also partly attributed to the higher pressure used in the high current experiment, no quantitative relation can be determined between the current and the strength of the virtual anode from these two experiments.
Figure 5 shows the expected ion energy between the cathode center and edge, this expected ion energy increases the further the ions are from the cathode center. Even though Figure 19 also shows an increase inside the entirety of the cathode, more data points between the cathode center and edge are required to validate the expected velocity profile as shown in Figure 5.
It should be noted that the measured outward acceleration does not necessarily mean that there is a virtual anode in the center of the cathode. There might be other explanations for the outward accelerations. Literature research did not find any plausible explanations, but is should be kept in mind regardless.

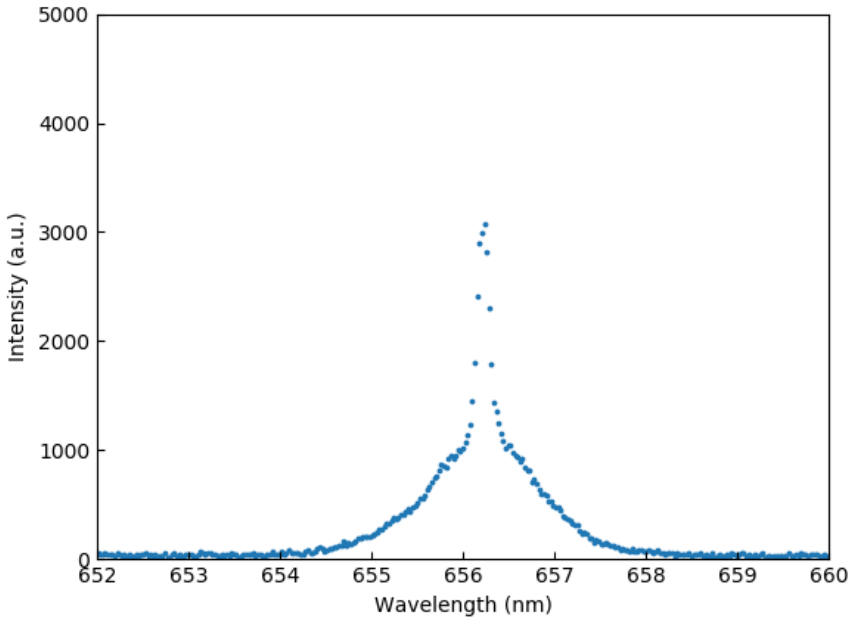

Figure 17: The spectrum measured using a current of 2 A (note that the vertical axis does not start at zero).

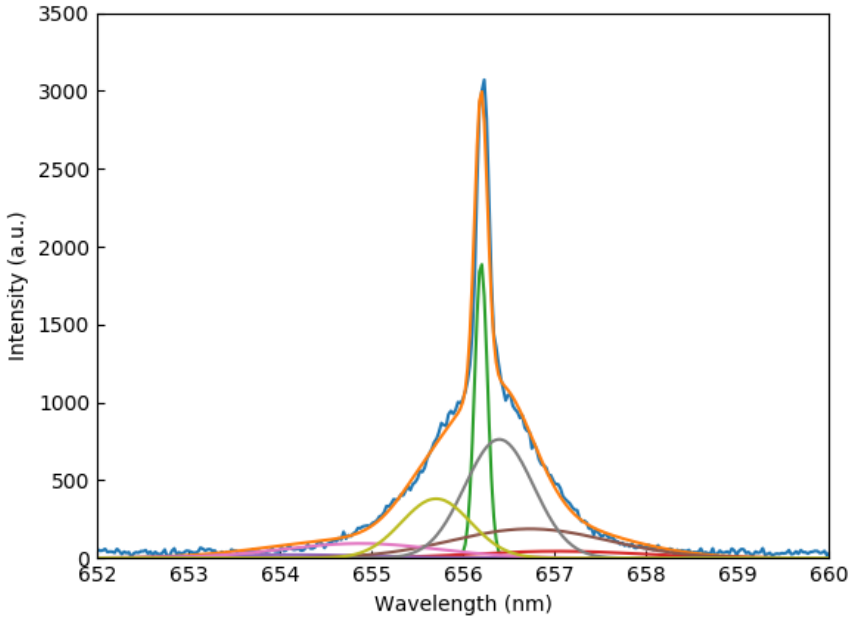

Figure 18: The spectrum at 23 mm in the star mode beam, fitted on Gaussian peaks corresponding to the expected Doppler shifts.

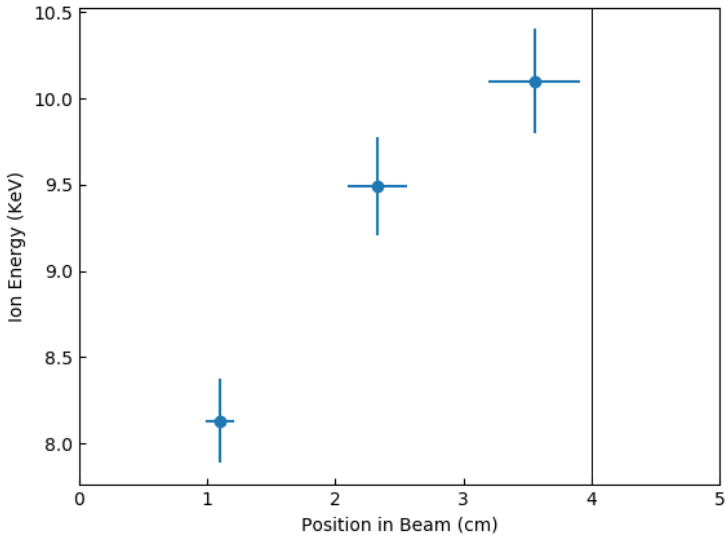

Figure 19: The energy of H^+ ions at different positions in the star mode beam using a current of 2 A.

4.5 Validity of the Measurements and Spectral Analysis

As mentioned before the error bars in Figure 16 are relatively big. The error bars in the horizontal axis are a direct effect of the shaking grid. During the measurements the grid shook a little bit, causing the star mode beam to move aswell. This means that the focus point of the optical system moved relatively to the beam, resulting in light from a different position in the star mode beam being measured. Due to the grid rotating slightly when it is shaking, the error in the measurement position gets bigger when measuring further from the grid center. This is because the star mode beam can turn towards or away from the optical path, which is an effect that scales with the distance from the grid center.
As described in Section 2.5 it takes some time before the excited neutrals decay. It is calculated that after 1 cm about 63 % of the neutrons have emitted a photon. For this reason all data points in Figures 16 and 19 represent the ion energy which was transferred to the neutral slightly before the emission of the photon. As this is a systematic error, this is not represented in the horizontal error bars.
The error bars on the vertical axis consist of two effects which both introduce an uncertainty. The first one is once again an artifact of the shaking grid, which resulted in the angle between the star mode beam and the optical path not being constant. This angle ϕ is used to calculate the energies shown in Figure 16 using equation 5. The second contribution to the vertical error bars comes from the fitting algorithm. It can be seen from both Figures 14 and 18 that the total fit, displayed as an orange line, does not perfectly match the data points, denoted in blue. Furthermore, the fitting algorithm approximates the H_2^+ and H_3^+ peaks as one $H_{2.5}^+$ peak and any slow ion peaks are also approximated as one peak. Also, the algorithm neglects any peaks which might arise due to background gas emitting photons. These uncertainties combined result in the vertical error bars as shown in Figures 16 and 19.

Initially, the ion energies as calculated in Figures 16 and 19 were lower than expected. The ion energies were expected to be closer to the acceleration voltage, which was 23 kV. However, the ions which were used to calculate the energies in these figures are accelerated by the virtual anode. Hence, it is to be expected that the radially outward moving ions do not have an energy of 23 KeV.

5 Conclusion

In this project the velocity of hydrogen ions in a fusor has been analysed. The velocity of the H^+ ions in a star mode beam has been measured at multiple locations using Doppler spectroscopy. The H^+ ions collide with atomic hydrogen, creating a fast moving excited neutral. The excited neutrals in turn emit a photon at the Balmer-alpha line, which is Doppler shifted due to the neutrals velocity. This Doppler shift has been used to calculate the velocity. A new optical system made it possible to determine the focus point with improved accuracy. The location of the star mode beam itself carried some inaccuracies, attributed to the shaking of the grid.

Measurements at different locations in the star mode beam were conducted using a low and a high current, being 20 mA and 2 A respectively. The low current measurements suggests an acceleration of the ions, but the error bars are to big for a definitive conclusion. It can therefore not be stated that there is a virtual anode present at a pressure of 0.2 pascal. The high current measurements show a clear ion acceleration. Figure 19 shows that the ion energy is increased between the cathode center and cathode edge. This increase proves that there is a virtual anode present inside the fusor at a pressure of 0.4 pascal. Experiments using a current of 2 A show a significantly larger acceleration, but as the pressure had to be increased to carry out those experiment, no conclusive statement can be made on whether the strength of the virtual anode increases with an increasing current.

At the University of Sydney a similar experiment has been conducted [7]. This experiment found results showing a radial outward acceleration inside the cathode, and no acceleration outside the cathode. The constant velocity outside the cathode is likely an artifact of the higher pressure used in the experiments carried out at the University of Sydney, namely between 1 and 2 Pa. The experiments in this project used a pressure of ≈ 0.2 Pa. The higher pressure means that the ions have a higher chance to collide earlier with background gas, meaning that their mean free path is shorter. A shorter mean free path results in less acceleration, and thus a smaller change in velocity.
The experiments done at the University of Sydney and during this project used similar acceleration voltages, namely 20 kV and 23 kV respectively. Therefore the difference in acceleration outside the cathode cannot be attributed to the voltage applied on the cathode.
Both the experiment conducted at the University of Sydney and the experiments conducted during this project found conclusive proof of a virtual anode being present at ≈ 1.5 pascal and 0.4 pascal respectively.

To conclude, the ion energy is found to increase between the grid center and grid edge, meaning that an accelerating force is working on the ions inside the grid. This accelerating force comes from a virtual anode, which is created due to the hollow cathode effect. The ion acceleration did increase significantly when using a higher current, but no decisive conclusion on the relation between the current and virtual anode can be drawn from this particular experiment due to the pressure being changed. The ion energy was expected to show a profile with a maximal acceleration at the center of the cathode as seen in Figure 5. This can not be verified with the limited amount of data acquired in this experiment.
The initial goal of this experiment was to determine whether a virtual anode influences ion motion inside a fusor at low pressures. The results of this experiment decisively confirm this for pressures as low as 0.4 pascal. Using this information, future research is required to determine the significance of this virtual anode with respect to neutron production. Depending on this research fusors can be optimized to utilize the virtual anode in favour of neutron production.

6 Future Research

Based on the results found in this experiment, the goal of future research should be to quantify the significance of the virtual anode and to determine the relation between the strength of the virtual anode and other parameters. The experiments in this project suggest that the virtual anode gets stronger with an increasing current, but this has to be validated by experiments which keep all other variables constant. Once these relations have been determined, settings can be found which maximize the strength of the virtual anode. Measurements using these settings can determine the significance of the virtual anode in neutron production. If these measurements show that the virtual anode does increase the neutron production, fusors can be optimized to utilize the virtual anode.

During the later stages of this project, possible improvements on the experimental set-up were devised which could not be implemented in the project itself. This chapter will discuss these possible improvements and how they might affect future research using a similar experimental equipment. Section 6.1 explains how the experimental set-up might be altered to achieve higher ion energies, and thus clearer spectra. Section 6.2 discusses how the focus point can be fixed in the star mode beam with a higher degree of certainty by using a different grid.

6.1 Improving the Spectral Measurements

As stated in Chapter 4 the H_2^+ and H_3^+ peaks could not be distinguished form one another in the measured spectra. This is mainly attributed to the spectra being too 'narrow', resulting in the peaks being pushed together. A broader spectrum is obtained when the light has a larger Doppler shift, meaning a higher energy of the ions is required.
The ion energy can be increased by increasing the voltage which is being applied to the cathode. Increasing the voltage usually goes together with a decrease in the pressure. If this decrease in pressure is too drastic, the plasma will cease to exist. This means that at a certain point the voltage cannot be increased anymore. The addition of an ion source can help facilitate higher voltages, as it directly injects ions into the vacuum chamber. The usage of this ion source would therefore be beneficial to the measurements, as it means the voltage can be increased. The more energetic ions will then result in the peaks in the spectra being further apart.
In this project the use of an ion source was discarded, as the ion source was located directly opposite to the optical set-up observatory port. The ion source therefore influenced the data as shown in Figure 11.
The influence of the ion source can be minimalised by placing it at an observatory port which is perpendicular to the observatory port from the optical set-up. This will result in the ions from the ion source moving in a beam which is perpendicular to the observatory port on which the optical system is mounted. The optical system can then be used to measure along a star mode beam which is not close to the beam generated by the ion source. This was not possible in the current project, as the location of the ion source caused the ions from the ion source to hit the optical system directly.
The same effect could be achieved by changing the location of the optical system, as long as the ion source and optical system are placed perpendicularly on the observatory ports. For the fusor at the TU/e, however, the size of the different observatory ports has to be taken into account. Therefore changing the location of the ion source is a more practical solution.

6.2 Targeting the Star Mode Beam

The optical set-up described in Section 3.2 provides the possibility to measure spectra inside the fusor at location determined within millimeter accuracy. Also, these measurements can be reproduced as this set-up is rigidly mounted on the fusor. The optical system can translate the focus point in three

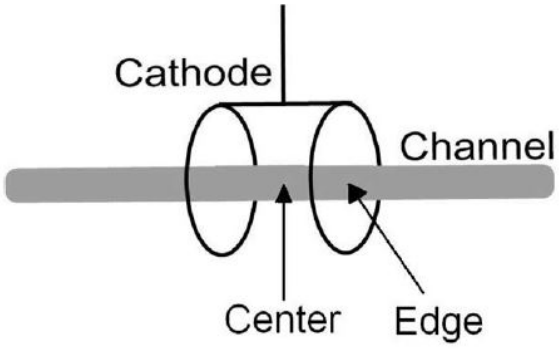

Figure 20: A grid build from two circular wires, connected by a horizontal wire. This grid poses certain advantages over the spherical grid when considering diagnostic purposes.

directions and can therefore scan a significant portion of the inside of the vacuum chamber. Yet, aiming the focus point in the star mode beam was found to be an obstacle during this project.
This difficulty was caused by the star mode beam itself. During the measurements, the cathode started shaking when higher voltages were applied to it. As the grid started shaking, the star mode beam started moving, while the optical system was aimed at one fixed location.
On top of this, the location of the star mode beam could not be determined exactly. An attempt was made to develop a theoretical model to locate the beam. But as not all the physics involving the star mode beam in this grid is yet understood, this model relied on assumptions which resulted in a big error. Therefore, a picture of the inside of the vacuum chamber was taken during operation, and the beam was located using this picture.
Both these problems can be solved using a grid designed by Shrier et al. as shown in Figure 20, this grid consists of two circular wires which are placed parallel [11]. As this grid is mounted to the stalk using the horizontal wire shown in Figure 20 it can be assembled in a fixed position. This was harder to do with a spherical grid, as a spherical grid has to be attached to the stalk using an extra wire, which does not prevent the spherical grid from rotating.
As can be seen in Figure 20 this grid only results in two beams which exit the cathode. A theoretical model for the locations of these beams is far more simplistic than a model for the beams in a spherical grid, as the only asymmetric effect that has to be taken into account is the horizontal wire connecting the two parallel rings.
The combination of a better understanding of the location of the beam and the limited movement of the cathode determines the position of the beam during the measurement with better accuracy than when using a spherical grid. Making it possible to measure along the beam with greater certainty. This eliminates a lot of checks which had to be conducted during this project and reduces the error bars.
When measuring spectra in the beams generated by the grid in Figure 20 it is possible to achieve a great variety of measurement angles, as the stalk can be rotated by a fixed angle, rotating the beams with the same angle. As there are hardly any grid wires obstructing measurements inside the cathode itself, it is possible to get a detailed ion velocity profile for the entire beam.
It should be noted that the proposed grid has possible disadvantages over spherical grids. One of these disadvantages might be that the neutron production rate drops significantly as the spherical symmetry is replaced by a cylindrical one. For the diagnostic purpose of determining the ion velocity in this project this is, however, an irrelevant disadvantage.

Implementing the above mentioned improvements allows for more accurate results. Using this improved experimental set-up and the fact that the virtual anode is proven to be present at low pressures, the finer details of the hollow cathode effect can be explored in future research. In doing so, fusors can be optimized to increase neutron production and in turn, be used to improve cancer treatment.

References

[1] N. Cardozo, "Fusion on the back of an envelope," p. ii, 2016.

[2] K. Ikeda, "Progress in the iter physics basics," *Nucl. Fusion*, vol. 47, 2007.

[3] T. Rider, "Fundamental limitations on plasma fusion systems not in thermodynamic equilibrium."

[4] R. Lawson *et al.*, "Neutrons in medicine," *phys. technol.*, vol. 13, 1982.

[5] T. Thorson *et al.*, "Fusion reactivity characterization of a spherically convergent ion focus," *Nuclear Fusion IAEA*, vol. 38.

[6] J. Kipritidis and J. Khachan, "Application of doppler spectroscopy in h_2 to the prediction of experimental $d(d,n)^3he$ reaction rates in an inertial electrostatic confinement device." *Physical review*, vol. E 79.

[7] J. Hermens, "Analysis of deuterium ion motion with doppler spectroscopy in an inertial electrostatic confinement device. report eindhoven university of technology," 2019.

[8] G. McClure, "Differential angular distribution of h and h^+ dissociation fragments of fast h_2^+ ions incident on h_2 gas." *Phys. Rev.*, vol. 140.

[9] A. Wolf, "Measurement of ion velocities in the tu/e fusor plasma using lif spectroscopy. master thesis eindhoven university of technology," p. 7, 2015.

[10] "Image courtesty: Michaël van witsen, tu/e."

[11] O. Shrier *et al.*, "Diverging ion mition in an inertial electrostatic confinement discharge." *Phys. Plasmas 13, 012703 (2006); https://doi.org/10.1063/1.2167584.*

[12] M. Fitzgerald, J. Khachan, and S. Bosi, "Relative densities of hydrogen ion species in a hollow cathode glow discharge," *The European Physics Journal D-Atomic, Molecular, Optical and Plasma Physics*, vol. 39, no. 1, pp. 35–39, 2006.

[13] J. Khachan and S. Collis, "Measurements of ion energy distributions by doppler shift spectroscopy in an intertial electrostatic confinement device," *Physics of Plasmas*, vol. 8, no. 4, pp. 1299–1304, 2001.

[14] U. S. department of commerce, "Atomic transition probabilities hydrogen through neon," *National Bureau of Standards*, vol. 1, p. 2, 1966.

[15] I. Williams *et al.*, "Balmer-alpha emission in collisions of h, h+, h2+ and h3+ with h2," *Journal of Physics B: Atomic and Molecular Physics*, vol. 15, no. 9, p. 1377, 1982.

[16] M. van Witsen, "Temperature control with pulsed power: Investigating surface fusion at the tu/e fusor grid. master thesis eindhoven university of technology," 2019.

[17] "Andor shamrock 500i specifications."

[18] M. Smathers, "How does a spectrometer work?" *Sciencing*, 2017.

[19] J. Kipritidis *et al.*, "Absolute densities of energetic hydrogen ion species in an abnormal hollow cathode discharge," *Physical review*, vol. E 77.